Nanostructured surfaces yield earlier: Molecular dynamics study of nanoindentation into adatom islands

Gerolf Ziegenhain and Herbert M. Urbassek*
Fachbereich Physik und Forschungszentrum OPTIMAS, Universität Kaiserslautern, Erwin-Schrödinger-Straße, D-67663 Kaiserslautern, Germany
(Received 1 March 2010; revised manuscript received 2 April 2010; published 29 April 2010)

Using molecular-dynamics simulation we investigate nanoindentation into an fcc metal surface covered by an adatom island. Small islands are pushed into the solid and transported away by prismatic dislocation loops, and no defects remain under the indenter; thereafter indentation proceeds as for a flat surface. For large islands, the island boundaries do not influence indentation. Most interesting is the intermediate case, where the island size is comparable to the contact radius of the indenter at the onset of plasticity. Here plasticity starts immediately at the surface under the weakest step edges bounding the island. The dislocations are pinned to the step edges and dislocation activity remains localized under the island. For this intermediate case, the surface is weakest and yields earliest.

DOI: 10.1103/PhysRevB.81.155456 PACS number(s): 62.20.F−, 68.35.Gy, 81.40.Lm, 62.20.Qp

I. INTRODUCTION

The physics underlying indentation into a flat surface is well understood.[1,2] Already in 1882, Hertz[3] found the basic relation between the indentation force F_{ind} and the elastic indentation depth d,

$$F_{\mathrm{ind}} = \frac{4}{3} E_r d^{3/2} \sqrt{R_{\mathrm{ind}}}. \tag{1}$$

In this relation, besides the indenter radius R_{ind}, only a single materials parameter, the so-called indentation modulus E_r enters.[1–4] For a rigid indenter, it may be expressed in terms of the Young's modulus E and the Poisson ratio ν of the substrate as

$$E_r = \frac{E}{1-\nu^2}. \tag{2}$$

Hertz also determined the contact area between indenter and substrate; when projected into the surface plane it is of circular shape with radius

$$r_c = \frac{3\pi}{4} \frac{p_c}{E_r} R_{\mathrm{ind}}. \tag{3}$$

The contact pressure p_c is defined by the ratio of the normal force F_{ind} divided by the contact area projected into the surface plane. Hertz obtained

$$p_c = \frac{4}{3\pi} E_r \sqrt{\frac{d}{R_{\mathrm{ind}}}}. \tag{4}$$

Hertz' analysis is valid in the elastic regime. As soon as the contact pressure surpasses the yield strength σ_c of the material, defects are created in the material and plastic yield sets in.

Nowadays, nanoindentation experiments can be performed into single crystals,[5,6] and also at specific surface defects. Here ground-breaking work has been performed by Kiely *et al.*,[7] who indented into and in the vicinity of surface steps. They showed that on single-crystalline Au surfaces, the yield stress is diminished at a step by 30%–45% relative to the flat terrace, and that the spatial zone of influence of the step extends to approximately 3 times the contact radius at the yield threshold, r_c^*. Molecular-dynamics simulation could corroborate these results,[8] but found a smaller spatial influence zone of the step, only $1.5r_c^*$. These authors also provide a model, which takes the direct contact of the indenter—when indenting into the lower terrace—with the step edge into account. It predicts an influence zone of $1.9r_c^*$, more compatible with the experimental result. More recent experimental and simulational work extends these results to vicinal surfaces, in which the surface structure provides for a regular array of parallel steps.[9] Another simulational investigation of relevance to our paper reports on the influence of a grain boundary intersecting a free surface on nanoindentation.[10] It showed that when indenting close to the boundary (distance smaller than the indenter radius) the yield stress is diminished and dislocations are nucleated at the boundary.

We want to extend here these previous studies and consider nanoindentation into a more complex surface defect than a surface step: Adatom islands are generic features on surfaces.[11] They constitute a new monolayer covering a part of the surface and are bounded by surface steps. While on large islands, and for indentation sufficiently far away from the bounding step edges, we expect no new physics, it is not clear how small islands will behave under nanoindentation. We shall investigate this question here using atomistic simulation.

II. SYSTEM

Cu is described using the many-body interatomic interaction potential developed by Mishin *et al.*[12] This potential is known to reproduce well the elastic properties, the stacking fault energies, which are important to describe plasticity,[13] and also the deformation paths.[14] The fcc substrate has approximately cubic shape with side lengths of around 25 nm; it contains 1.35×10^6 atoms. We checked in a series of simulations that our crystallite size is large enough to obtain reliable results for the indentation process. Lateral periodic boundary conditions have been applied. At the bottom, atoms

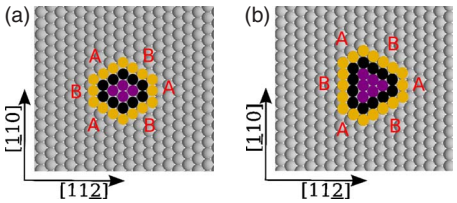

FIG. 1. (Color online) Schematics of the two forms of adatom islands used for nanoindentation. The island core is colored in purple (dark gray) and characterized by the island size $S=1$. S counts the number of additional rings around the core; the displayed islands have $S=3$. The A and B steps bordering the islands are indicated. (a) island type 1, (b) type 2.

in a layer of width 10 Å have been constrained to $F_{\text{normal}}=0$.

The crystal has a (111) surface. Adatom islands of roughly hexagonal shape are laid on it according to 2 different schemes, cf. Fig. 1. The boundary of an island is formed by surface steps. When the step edge runs along the ⟨110⟩ orientation, two different steps can result; the A-step forms a local {100} microfacet, and the B-step a local {111} microfacet, see Fig. 1. For Cu, the energetic difference between the A- and B-steps bounding the island is only around 1%;[11,15] hence both steps appear with roughly equal side lengths. Note that real islands obey a threefold symmetry with rounded corners; their shape fluctuates due to temperature.[11] We simulated two types of islands in order to investigate the influence of island shape. The entire crystal, including the adatom island, is carefully relaxed before starting the indentation in order to relieve all stress inside the material. The simulations are performed at 0 K, since we are interested in the fundamental mechanisms of plasticity generation, and it is known that the thermal energy is not sufficient to initiate plasticity on the time scales of a molecular-dynamics simulation.[16]

Islands are characterized by the number of rings S of adatoms around the island core, which are needed for their construction, cf. Figure 1. We study islands with $S=1-20$. The total number of atoms in an island of size S amounts to

$$N = 3S^2 + S, \tag{5}$$

for type 1, and $2S$ more for type 2. For our discussion it will be useful to define an effective island radius r_{island}. This may be done by counting the area of the island, $A=NA_{\text{atom}}$, and equate it to πr_{island}^2. Here $A_{\text{atom}}=(\sqrt{3}/2)r_{\text{NN}}^2=5.66$ Å^2 is the surface area occupied by an adatom, and $r_{\text{NN}}=2.556$ Å is the nearest-neighbor distance in Cu. This procedure gives

$$r_{\text{island}} \cong \sqrt{\frac{3\sqrt{3}}{2\pi}} S r_{\text{NN}} \cong 0.91 S r_{\text{NN}} \tag{6}$$

for both island types. In this formula, only the quadratic term $N=3S^2$ of Eq. (5) has been used. We note that other definitions of r_{island}, e.g., with the help of the cluster periphery, give results within a few percent of Eq. (6). Islands of type 2 possess the threefold symmetry of the (111) surface, while islands of type 1 are of lower symmetry.

The indenter is modeled as a repulsive sphere. We chose a non-atomistic representation of the indenter, for which its interaction potential with the substrate atoms is described by[17]

$$V(r) = \begin{cases} k(R_{\text{ind}} - r)^3, & r < R_{\text{ind}}, \\ 0, & r \geq R_{\text{ind}}. \end{cases} \tag{7}$$

We study two values of the indenter radius, $R_{\text{ind}}=8$ and 4 nm. As in previous work,[13] the indenter stiffness is set to $k=3$ eV/Å^3. We checked that our results are only weakly influenced by the exact value of the indenter stiffness, as long as it is in the range of 1–10 eV/Å^3.

The simulations have been performed using a modified version of the LAMMPS code,[18] using the so-called displacement-controlled approach.[19,20] The indenter is advanced every $\Delta t=2$ ps by a fixed amount of $\delta=0.256$ Å (≪lattice constant) instantaneously, corresponding to an average indentation speed of $v=12.8$ m/s. The substrate then relaxes for the ensuing time of Δt to the new indenter position.

For defect identification we use the angular distribution method devised by Ackland and Jones.[21] It differentiates between atoms in an undisturbed fcc neighborhood, atoms in a local hcp neighborhood (stacking fault), and others. We define the defect concentration x_{sf} as the relative number of atoms in stacking faults relative to the total number of substrate atoms.

III. RESULTS

A. Steps

We shall investigate the response of three types of steps to nanoindentation. A and B steps, which bound the islands considered here, have already been introduced in Sec. II above. These steps run along the ⟨110⟩ orientation. We shall also consider a third kind of step occurring on fcc (111) surfaces, in which the step edge runs along the $[11\bar{2}]$ direction. Here, each step atom forms a kink, and the step is called an open fully kinked step, or briefly kink step.

Indentation onto the periphery of a (larger) island will be equivalent to indenting a step edge. In our islands, only A and B steps occur. While indentation of steps has already been studied previously,[8,9] we shall focus here on characterizing the yield strength of the steps. We may view the upper terrace of the step as the (large) island, and the lower terrace as the substrate.

Figure 2(a) displays the force F_{ind} on the indenter as a function of the indentation depth d when indenting with the 8-nm indenter directly onto the step edge. Results for the defect concentration, x_{sf}, and the contact pressure, p_c, are shown as well. Indentation of an ideal, step-free (111) surface is included as a reference. For all 3 steps we observe a small first load drop at $d=3-7$ Å, which is accompanied by defect formation, Fig. 2(c). The defects are formed immediately at the step edge; this nucleation mechanism has been termed *heterogeneous*. This is in contrast to defect formation by nanoindentation of a flat terrace, where dislocations nucleate in the bulk material under the indenter at the posi-

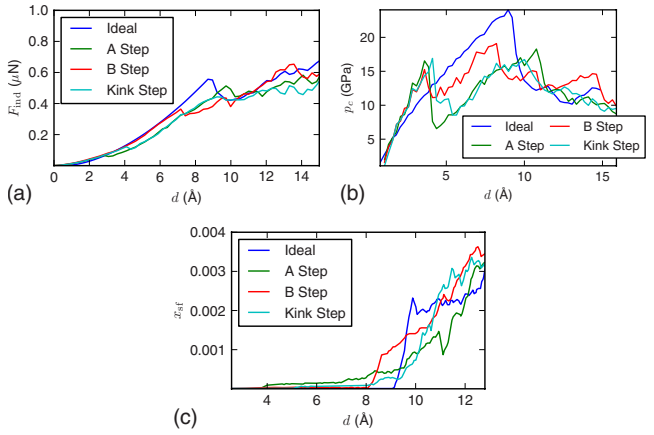

FIG. 2. (Color online) Nanoindentation into a surface step with an indenter of 8 nm radius. Evolution of (a) indenter force $F_{\rm ind}$, (b) contact pressure p_c, and (c) defect concentration $x_{\rm sf}$ with indentation depth d.

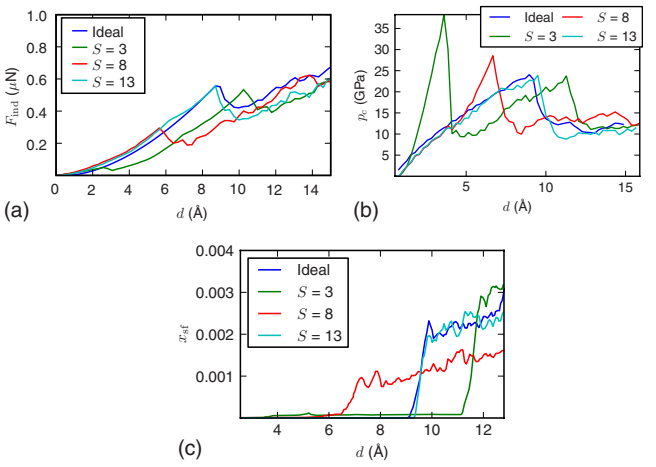

FIG. 3. (Color online) Nanoindentation into adatom islands. Evolution of (a) indenter force $F_{\rm ind}$, (b) contact pressure p_c, and (c) defect concentration $x_{\rm sf}$ with indentation depth d.

tion of highest resolved shear stress; this nucleation mechanism has been termed *homogeneous*.[9,22–25]

A second load drop occurs at $d=7-10$ Å. While the first load drop corresponds to the formation of defects at the step edge, the second, more severe load drop occurs when the indenter also touches the lower terrace; this event marks the onset of full plastic activity. The essential message of Fig. 2(a) is that both the first and the second load drop occur first in the A step, then in the kink step and finally in the B step. We thus conclude that the A step is the weakest and the B step the strongest of the 3 steps investigated here.

Figure 2(b) demonstrates that the contact pressures needed to induce plasticity in the upper terrace of the stepped surfaces are about 64%–70% of the strength of the ideal surface; note that also the lower terrace (second yield point) does not require much more pressure to yield. The yield strengths of the three steps are about the same.

B. Islands

When indenting into islands, we position the indenter into the middle of the island. Only islands of type 1 will be discussed here; the results for islands of type 2 are analogous and will be summarized in Sec. III C below. Figure 3 shows the results for islands of different sizes.

The ideal surface shows no defects until the load drop occurs at $d=8.8$ Å at a contact pressure of 24.2 GPa; then the number of defects rises steeply indicating the formation of extended dislocation loops. For a large island ($S=13$), the results are analogous. For small islands ($S=1-3$), the situation is very different: after a small load drop occurring at $d=1.7$ Å, the force returns to the Hertzian behavior, albeit shifted toward larger depths. The pressure exhibits a strong maximum at this early load drop, which is due to the very small contact area (equal to the island area). Note that (almost) no defects have been generated after this load drop. Intermediate island sizes ($S=8$) show the most complex behavior: an early load drop at an indentation depth of 6 Å, somewhat smaller than for the ideal surface, induces abundant defect generation. We shall discuss the 3 regimes of island sizes in more detail, using atomistic representations of the plasticity generated.

1. Small islands

The plasticity generated for $S=3$ islands is visualized in Fig. 4. Immediately after the initial load drop a dislocation loop has formed. The loop moves away from the indenter into the substrate, Fig. 4(a), while the surface looks virgin under the indenter. This means that the island has been pushed as a whole into the substrate and is transported away from beneath the indenter. The establishment of a defect-free surface is also the reason why after the early load drop, the force-displacement curve, Fig. 3(a), resembles the undisturbed elastic Hertzian curve; it is only shifted by 1 monolayer ($\Delta=2.08$ Å) into the substrate. After the removal of the island, no defects have remained under the indenter.

Plastic yield of the substrate then happens at an indenter distance, which is a distance Δ deeper than for the virgin

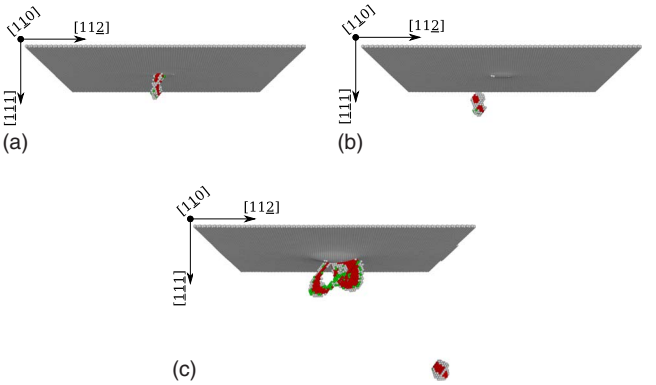

FIG. 4. (Color online) Plasticity below a small island ($S=3$) at indentation depths of $d=3.8$ Å (a), $d=5.4$ Å (b), and $d=11.2$ Å (c). The plots show a perspective side view, which can be identified by the axes drawn. The gray area shows the surface. The atoms colored in red (dark gray) display dislocation loops.

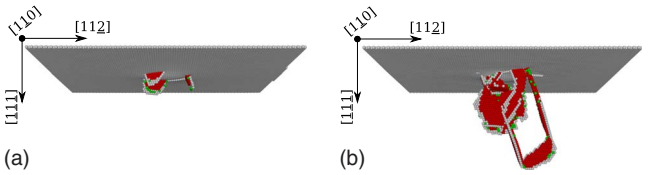

FIG. 5. (Color online) Plasticity below a midsize island ($S=10$) at indentation depths of $d=7.4$ Å (a), and $d=9.4$ Å (b).

surface. The generated plasticity looks identical to that[13] produced for the ideal surface.

2. Midsize islands

For the example of $S=10$, Fig. 5 shows the development of defect generation. After the first load drop at around $d=6$ Å, Fig. 3(a), dislocation loops are generated at the A steps of the island. This is understandable from the fact that these steps are weakest, cf. Figure 2. Thus defect formation is heterogeneous and starts at the (A) step edges; during the ensuing indentation the stacking faults remain pinned at the edges during the entire simulation time. We did not observe a second load drop for these mid-size islands.

3. Large islands

For $S>10$, plasticity starts homogeneously below the indenter in the middle of the island, and no longer at the step edges; Fig. 6. However, as soon as the evolving stacking faults grow into the vicinity of the island edges, they are attracted and pinned there. We observe that during the course of our simulation the plasticity remains localized below the island, and does not grow laterally.

C. Dependence on island size: role of critical contact radius

In this section, we wish to explore quantitatively the dependence of plasticity on island size. For this purpose let us define r_c^* as the critical contact radius of the indenter with the material at the moment where plastic deformation sets in. We identify it by the criterion that $x_{sf}>0$.

Figure 7(a) demonstrates that for small islands, the critical contact radius r_c^* is

$$r_c^* = r_{\text{island}}. \tag{8}$$

This is understandable as it shows that the indenter entirely contacts the island before the onset of plasticity.

Beyond a threshold island size, r_c^* becomes independent of r_{island}; in this case r_c^* evidently assumes the value valid for a flat terrace, $r_c^{*,\infty}$. Hertz' theory shows that $r_c^{*,\infty}$ is given by

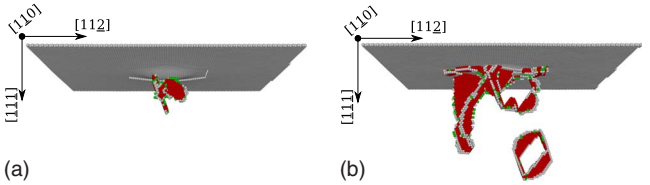

FIG. 6. (Color online) Plasticity below a large island ($S=20$) at indentation depths of $d=9.4$ Å (a), and $d=10.3$ Å (b).

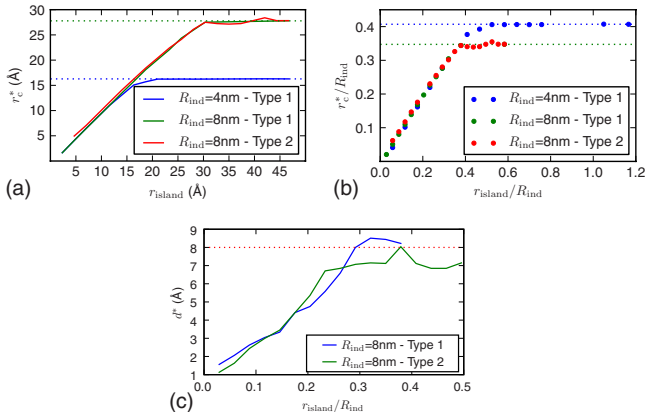

FIG. 7. (Color online) Synopsis of indentation into adatom islands of various sizes. (a) Contact radius at onset of plasticity, r_c^*, vs island size, r_{island}. The black line indicates proportionality according to Eq. (8). The horizontal dotted lines indicate the values of the contact radii r_c^* for large islands, which can be compared to the analytical estimate, Eq. (9). (b) Same data scaled to indenter radius R_{ind}. (c) Indentation depth at onset of plasticity, d^*. The dotted line indicates a value of $d^*=8$ Å, as expected for a flat terrace, see text.

Eq. (3), when the contact pressure reaches the yield strength, σ_c,

$$r_c^{*,\infty} = \frac{3\pi}{4}\frac{\sigma_c}{E_r}R_{\text{ind}}. \tag{9}$$

We may use the yield strength $\sigma_c=24.2$ GPa, Fig. 3, and the indentation modulus $E_r=152-192$ GPa for the Cu(111) surface.[26] The lower value stems from a calculation using linear anisotropic elastic theory, while the higher value stems from a fit of the Hertzian force-displacement curve to Hertz' law; the deviations are due to nonlinear elastic stiffening of the material under load. Using these materials parameters, we obtain from Eq. (9) that $r_c^{*,\infty}=(0.30-0.38)R_{\text{ind}}$. Figure 7(b), where our simulation results are scaled to the indenter radius R_{ind}, demonstrates that this analytical estimate is in fine agreement with our simulation result.

Our main conclusion is hence that islands which are larger than

$$r_{\text{island}} > \beta R_{\text{ind}} \tag{10}$$

behave like a flat surface. Here β is given by the prefactor in Eq. (9) and is $\beta\cong 0.4$ for Cu. Smaller islands are weakened in the sense that they yield already for smaller indentation forces.

This result is in agreement with earlier studies on nanoindentation of a step[7,8] which showed that the step has only an influence if the critical contact radius $r_c^*>D$, where D is the distance of the indenter to the step edge. As described in Sect. I, these earlier studies even found an influence of the step, if r_c^* is (up to a factor of 3) smaller than D; this is not corroborated by our simulations. In our case, the condition $r_c^*>D$ translates into $r_c^*>r_{\text{island}}$ since we indent into the middle of the island; in this argument we assume that step curvature plays no role.

We performed all our simulations for two different island forms as sketched in Fig. 1. Our results summarized in Fig. 7(a) demonstrate that elastic indentation and onset of plasticity are independent of island type.

Finally, Fig. 7(c) displays the dependence of the indentation depth at yield, d^*, versus island size. We see that d^* increases approximately linearly with island size, until it saturates at roughly that island size that corresponds to the saturation of the contact radius, Eq. (10).

Inserting the yield strength $\sigma_c = 24.2$ GPa and $E_r = 152–192$ GPa, as above, Eq. (4) gives a critical indentation depth of $d^* = (0.09–0.14)R_{\mathrm{ind}}$, which amounts to 7–11 Å for a 8-nm indenter. Figure 7(c) shows that this is in reasonable agreement with our simulation results for large islands.

IV. CONCLUSIONS

Defects at the surface, such as surface steps and adatom islands, weaken the surface such that they yield earlier than a flat terrace. In the case of adatom islands, which have been investigated in this paper, the island size—relative to the indenter radius—matters. Large islands ($r_{\mathrm{island}} > \beta R_{\mathrm{ind}}$ with $\beta \cong 0.4$ in the case of Cu studied here) behave like a flat terrace, if indented in the center of the island. Smaller islands are weakened, since the contact radius of the indenter at the point of plastic yield reaches the island boundaries. Dislocations are nucleated immediately at the surface under the weakest step edges bounding the island; these are the A steps. The dislocations are pinned to the step edges and dislocation activity remains localized under the island. For this intermediate case, the surface is weakest and yields earliest. The smallest islands (in our case, comprising only up to 30 atoms) behave still differently under nanoindentation: they are pushed into the solid and transported away by prismatic dislocation loops, and no defects remain under the indenter; thereafter indentation proceeds as for a flat surface.

ACKNOWLEDGMENTS

The authors acknowledge financial support by the Deutsche Forschungsgemeinschaft via the Graduiertenkolleg 814.

*urbassek@rhrk.uni-kl.de; http://www.physik.uni-kl.de/urbassek/

[1] A. C. Fischer-Cripps, *Nanoindentation*, 2nd ed. (Springer, New York, 2004).
[2] A. C. Fischer-Cripps, *Introduction to Contact Mechanics*, 2nd ed. (Springer, New York, 2007).
[3] H. Hertz, J. Reine Angew. Math. **92**, 156 (1882).
[4] L. D. Landau and E. M. Lifshitz, *Theory of Elasticity*, 2nd ed., Course of Theoretical Physics Vol. 7 (Pergamon, Oxford, 1970).
[5] J. D. Kiely and J. E. Houston, Phys. Rev. B **57**, 12588 (1998).
[6] J. D. Kiely, K. F. Jarausch, J. E. Houston, and P. E. Russell, J. Mater. Res. **14**, 2219 (1999).
[7] J. D. Kiely, R. Q. Hwang, and J. E. Houston, Phys. Rev. Lett. **81**, 4424 (1998).
[8] J. A. Zimmerman, C. L. Kelchner, P. A. Klein, J. C. Hamilton, and S. M. Foiles, Phys. Rev. Lett. **87**, 165507 (2001).
[9] V. Navarro, O. R. de la Fuente, A. Mascaraque, and J. M. Rojo, Phys. Rev. Lett. **100**, 105504 (2008).
[10] E. T. Lilleodden, J. A. Zimmermann, S. M. Foiles, and W. D. Nix, J. Mech. Phys. Solids **51**, 901 (2003).
[11] T. Michely and J. Krug, *Islands, Mounds, and Atoms*, Springer Series in Surface Science Vol. 42 (Springer, Berlin, 2004).
[12] Y. Mishin, M. J. Mehl, D. A. Papaconstantopoulos, A. F. Voter, and J. D. Kress, Phys. Rev. B **63**, 224106 (2001).
[13] G. Ziegenhain, A. Hartmaier, and H. M. Urbassek, J. Mech. Phys. Solids **57**, 1514 (2009).
[14] S. Ogata, J. Li, and S. Yip, Science **298**, 807 (2002).
[15] C. Steimer, M. Giesen, L. Verheij, and H. Ibach, Phys. Rev. B **64**, 085416 (2001).
[16] G. Ziegenhain and H. M. Urbassek, Philos. Mag. **89**, 2225 (2009).
[17] C. L. Kelchner, S. J. Plimpton, and J. C. Hamilton, Phys. Rev. B **58**, 11085 (1998).
[18] http://lammps.sandia.gov/.
[19] D. Christopher, R. Smith, and A. Richter, Nucl. Instrum. Methods Phys. Res. B **180**, 117 (2001).
[20] X.-L. Ma and W. Yang, Nanotechnology **14**, 1208 (2003).
[21] G. J. Ackland and A. P. Jones, Phys. Rev. B **73**, 054104 (2006).
[22] T. Zhu, J. Li, K. J. Van Vliet, S. Ogata, S. Yip, and S. Suresh, J. Mech. Phys. Solids **52**, 691 (2004).
[23] M. A. Tschopp, D. E. Spearot, and D. L. McDowell, Modell. Simul. Mater. Sci. Eng. **15**, 693 (2007).
[24] X. H. Liu, J. F. Gu, Y. Shen, and C. F. Chen, Scr. Mater. **58**, 564 (2008).
[25] T. Zhu, J. Li, A. Samanta, A. Leach, and K. Gall, Phys. Rev. Lett. **100**, 025502 (2008).
[26] G. Ziegenhain, H. M. Urbassek, and A. Hartmaier, J. Appl. Phys. **107**, 061807 (2010).